Integrated Project (IP)
Project No. TIP5-CT-2006-031415

Thematic Priority 6:
Sustainable Development,
Global Change and Ecosystems

Recommendation of, and scientific basis for, optimisation of switches & crossings – part 1

INNOTRACK GUIDELINE

Deliverable report D3.1.5

Table of Contents

1. Executive Summary

The objective of INNOTRACK SP3.1 (task 3.1.6 Optimisation) is the development of innovative S&C (Switches & Crossings) designs that allow for increased axle loads and speeds and that lead to a decreased need for maintenance. The present report provides a guideline for the optimisation of geometry and support stiffness in the switch and crossing panels.

To meet these aims, simulation tools have been used to calculate wheel-rail contact forces, wheel-rail contact stresses, wear index and a rolling contact fatigue (RCF) index at key components in the S&C. As reported in INNOTRACK deliverable 3.1.4, these tools have been validated with respect to results from a field test.

Railway vehicles often experience significant lateral displacements, sometimes leading to wheel flange contact, when running in the switch panel. This leads to increased wheel and rail wear and sometimes RCF problems on the rails, requiring increased supervision and maintenance and reducing the life of the components.

To find means to improve the switch panel design, the geometry of a designed track gauge variation in the switch panel has been modelled in a parametric way. This was done for one type of turnout. For traffic in the facing and trailing moves of the through route, an optimum solution was identified and then validated by evaluating a wider set of simulation cases (different wheel profiles). The optimum design includes a 12 mm maximum gauge widening. The main benefits obtained by the proposed design are a significant reduction of wear along the switch panel and a significant reduction of traction coefficient, and therefore improved behaviour in terms of RCF. The methodology can be applied to other types of turnout designs.

Severe impact loads may be generated when wheels transfer between wing rail and crossing nose in the crossing panel. Thus, another objective has been to optimise the crossing geometry and the support stiffness of the superstructure in order to reduce the contact stresses induced by the wheels.

The numerical assessment of contact loads for a crossing panel with reduced support stiffness (by means of elastic rail pads) instead of

the standard support stiffness shows that impact loads can be reduced considerably especially for crossing negotiation at high speed. Investigations of different crossing geometries show that it is difficult to find a solution that leads to a force reduction for all wheel profiles occurring in service. Nevertheless, the MaKüDe crossing design showed the best performance for moderately worn wheel profiles in both running directions (facing and trailing moves). In combination with a reduced support stiffness, this crossing design will lead to a significant reduction of the impact loads and consequently has a high potential for LCC (Life Cycle Cost) reduction.

Field and laboratory testing of new S&C designs will be performed within INNOTRACK SP3. Some tests have started, whereas some are still being planned. To enable an assessment of the influence of the new designs on the long-term degradation of S&C, these field tests will not be finished and reported before the end of INNOTRACK. A report on results from field tests of different crossing designs at test site Haste in Germany will be reported in INNOTRACK deliverable 3.1.8 (due in December 2010). Results from field tests (Frankfurt and Wirtheim, Germany) of modified stiffness in the switch panel will be reported in INNOTRACK deliverable 3.19 (due in January 2011). Finally, the results from a field test (Eslöv, Sweden) of new S&C designs will be reported in INNOTRACK deliverable 3.1.10 (due in May 2011).

2. Introduction

The different components of a switch & crossing (S&C, turnout, point) are illustrated in Figure 2.1 [2.1]. The through and diverging routes are shown. Traffic in the facing move means that traffic is travelling from the switch panel to the crossing panel. Consequently, traffic in the trailing move means traffic travelling in the opposite direction.

Dynamics and damage of S&C are surveyed in the state-of-the-art report by Sällström et al [2.2]. Mathematical modelling, numerical simulation and field testing of dynamic vehicle–track interaction in S&C are treated by Kassa [2.3]. Statistics on the need for maintenance in S&C have been presented by Nissen [2.4].

INNOTRACK deliverable 3.1.4 contains a validation of the simulation models used here and a pre-report on the optimisation of S&C [2.5].

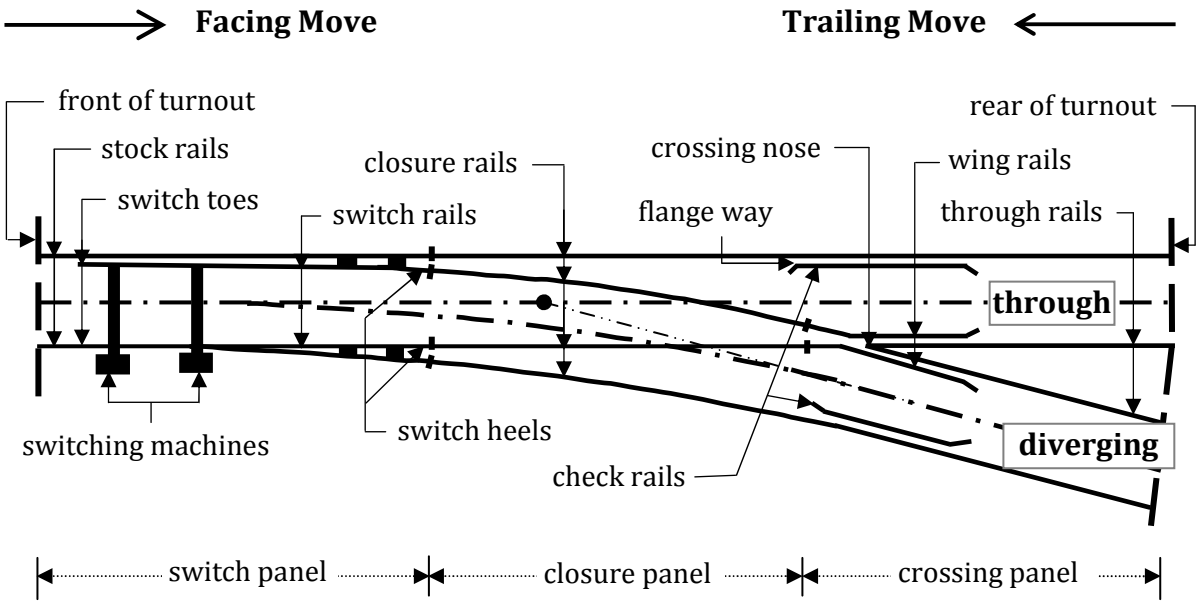

Figure 2.1. Components of a turnout with through and diverging routes. From [1]

The optimisation of stiffness and geometry in the switch panel was performed by Manchester Metropolitan University (Rail Technology Unit at the Department of Engineering and Technology). Section 3 in this guideline was written by Dr Elias Kassa. The optimisation of stiffness and geometry in the crossing panel was performed by Deutsche Bahn AG (Systemverbund Bahn, DB Systemtechnik). Section 4 in this guideline was written by Mr Dirk Nicklisch. The guideline was edited by Prof Jens Nielsen of Chalmers University of Technology (CHARMEC at the Department of Applied Mechanics).

2.1. Bibliography

2.1 E Kassa and J C O Nielsen, Dynamic interaction between train and railway turnout – full-scale field test and validation of simulation models. *Vehicle System Dynamics* Vol 46, Issue S1 & 2, 521-534, 2008

2.2 J H Sällström, T Dahlberg, M Ekh and J C O Nielsen, State-of-the art study on railway turnouts – dynamics and damage, Research Report, *Department of Applied Mechanics, Chalmers University of Technology,* Gothenburg, Sweden, 50 pp, 2002

2.3 E Kassa, Dynamic train–turnout interaction – mathematical modelling, numerical simulations and field testing, PhD thesis, *Department of Applied Mechanics, Chalmers University of Technology,* Gothenburg, Sweden, 2007

2.4 A Nissen, Analys av statistic om spårväxlars underhållsbehov (Analysis of statistics on the need for maintenance in switches & crossings, in Swedish), Licentiate Thesis, *Avdelning för drift och underhåll, Luleå Technical University, JvtC – Railway research centre*, Luleå, Sweden, 2005

2.5 J C O Nielsen (editor), Summary of results from simulations and optimisation of switches, INNOTRACK deliverable 3.1.4, 35 pp and 4 annexes, December 2008

3. Optimisation of geometry and stiffness in the switch panel

3.1. Background

In S&C, when a vehicle is running in the diverging route, large lateral wheelset displacements are developed leading to severe flange contact with the curved switch rail. This is mainly due to the abrupt change in track curvature and the large cant deficiency. It has also been observed that vehicles running on the through route in the switch panel often experience significant lateral wheelset displacements, sometimes leading to flange contact with the straight switch rail. These flange contacts result in an increase in wear of the switch rails and on some occasions in RCF problems on the rails, requiring increased inspection and maintenance and leading to reduced life of the components.

Simulations of a train passing an S&C in both routes, and in facing and trailing moves, have been performed using the MBS package SIMPACK to understand the underlying phenomena and to devise a strategy for the gauge optimisation process, see also [3.1]. A freight vehicle model, with a car body and two Y25 bogies, is used. In the simulations the vehicle model is allowed to run on a length of tangent track before entering the turnout which has constant curvature geometry. The optimisation process was performed for a standard S&C design (UIC60-760-1:15) with curve radius 760 m and turnout angle 1:15.

The rail cross-section varies continuously along the switch panel. At switch panel entry, there is only one full rail cross-section on each side of the track. Additional rails are then introduced on each side, with their cross-sections varying from a thin section at the switch toe to a full-sized rail cross-section at the switch heel. These additional rails lead to a continuous change in track stiffness, which has been shown by track receptance measurements at several locations in an S&C, see [3.2].

The objective has been to optimise the vertical track stiffness in the switch panel, possibly by adjusting the rail pad stiffness or by use of under sleeper pads. In this way, the abrupt changes in track stiffness,

due to the appearance of two rails and changes in rail cross-section, could be reduced and wheel-rail contact forces minimised. In addition, optimisation of track gauge at the switch panel entry, where the curvature changes abruptly, has been performed and the effectiveness of dynamic gauge widening techniques to reduce tangential contact forces and hence wear of the switch rail has been assessed.

3.2. Track gauge optimisation

To balance the artificial gauge increase generated due to the contact point trajectories in the switch panel, two possible dynamic gauge widening geometries are proposed, one for each route. The geometry is parameterised by three variables. It consists of four circular curves, see Figure 3.1. Dynamic gauge widening applies a continuous variation of the gauge by moving the stock rails laterally at the switch entry which results in a gauge increase. The optimisation process has been carried out using only one type of vehicle model, a freight vehicle model with Y25 bogies, and a typical wheel profile in the simulations. The optimised geometry was then evaluated with several load cases consisting of 18 different measured wheel profiles in terms of wear index, normal contact forces, RCF index and contact point position on the rail.

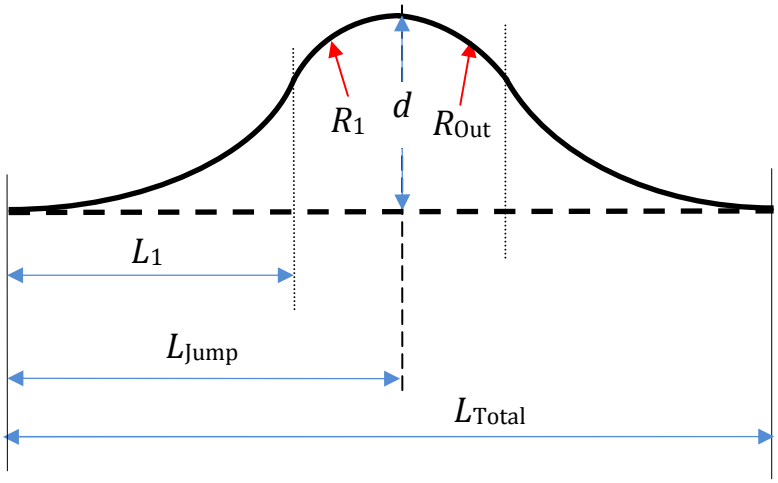

Figure 3.1. Gauge optimisation parameters

3.2.1. Through route

The geometry of the gauge variation is represented parametrically by three variables. For a more thorough discussion on the geometrical representation, see [3.3]. Finding an optimal design for the dynamic gauge widening is performed by varying the values of the maximum gauge widening amplitude. Several outputs were assessed to determine the optimal dynamic gauge widening geometry, see [3.1] for the full report. Here, some selected results from the study are discussed. Figure 3.2 shows the influence of different gauge widening amplitudes on the normal wheel-rail contact force. The results are compared with the nominal design. The smallest (8 mm) and the highest (20 mm) amplitude designs result in high transients between 8 to 8.5 m from switch entry. This happens when the load is fully transferred from a two-point contact (the first contact point is the contact on the stock rail whereas the second contact point is the contact on the switch rail) to a single-point contact on the switch rail. For the other studied gauge widening amplitudes, there is no significant change in the normal contact force before or after the contact jump. However, the appearance of the second contact point, contact on the switch rail, is delayed by 30 – 40 cm.

For the two contact points, the calculated wear indices along the switch panel for all levels of gauge widening amplitudes are shown in Figure 3.3. Wear index is calculated as the product of the creep forces and creepages in the longitudinal and lateral directions. It is observed that the application of a dynamic gauge widening leads to a reduction in wear index along the switch panel, and that the maximum value of the wear index is reduced considerably for gauge widening amplitudes 8 mm – 16 mm. However, the 20 mm gauge amplitude leads to an increase in wear index, and the reduction using the 18 mm gauge amplitude design is not significant compared to the other designs.

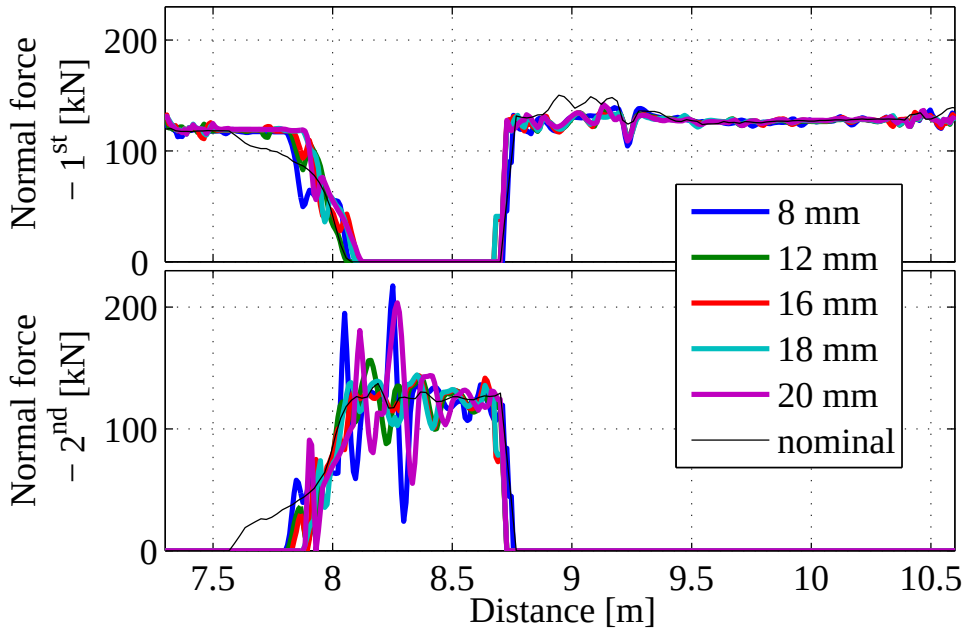

Figure 3.2. Wheel-rail normal contact force in the switch panel for different gauge widening amplitudes. First contact point (top), second contact point (bottom). Train in facing move of through route

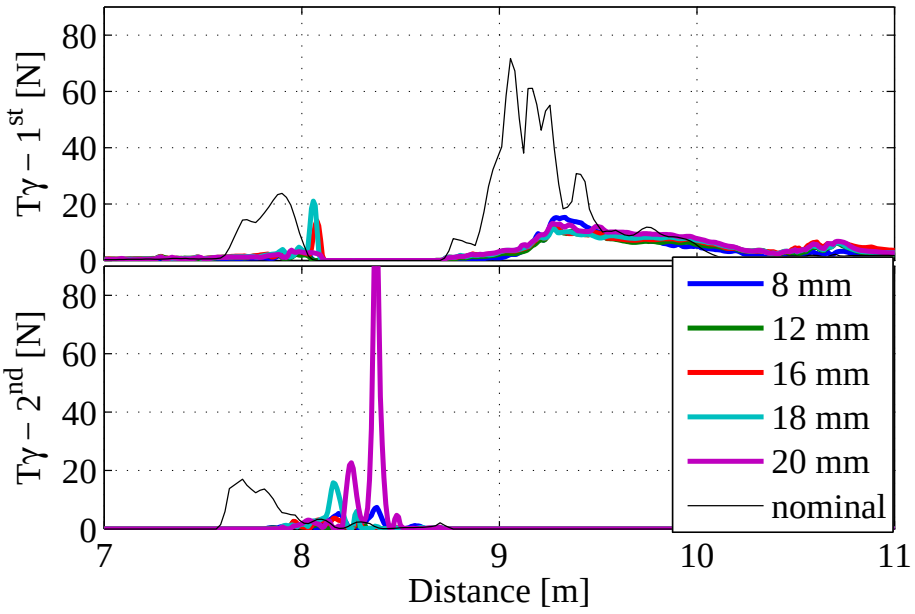

Figure 3.3. Wear index ($T\gamma$) in the switch panel for different gauge widening amplitudes. First contact point (top), second contact point (bottom). Train in facing move of through route

The two designs of dynamic gauge widening (12 mm and 16 mm), which proved to be optimal in the facing move, were subsequently evaluated in the trailing move with respect to wear index. Figure 3.4 shows the predicted wear indices in the switch panel for the trailing move with distance measured from the beginning of the S&C. For the 16 mm gauge widening, contrary to the facing move, the wear index is slightly increased both in the 1st and 2nd contacts. In addition, the location of the maximum wear index on the switch rail has shifted towards the switch toe, where the thickness of the switch rail is smaller. As in the case of the facing move, the 12 mm gauge widening amplitude leads to a significant improvement in reducing the wear index. Therefore, the design corresponding to the 12 mm maximum gauge widening is the optimal design both for the facing and trailing moves. For a more thorough discussion on other simulation outputs, see [3.1].

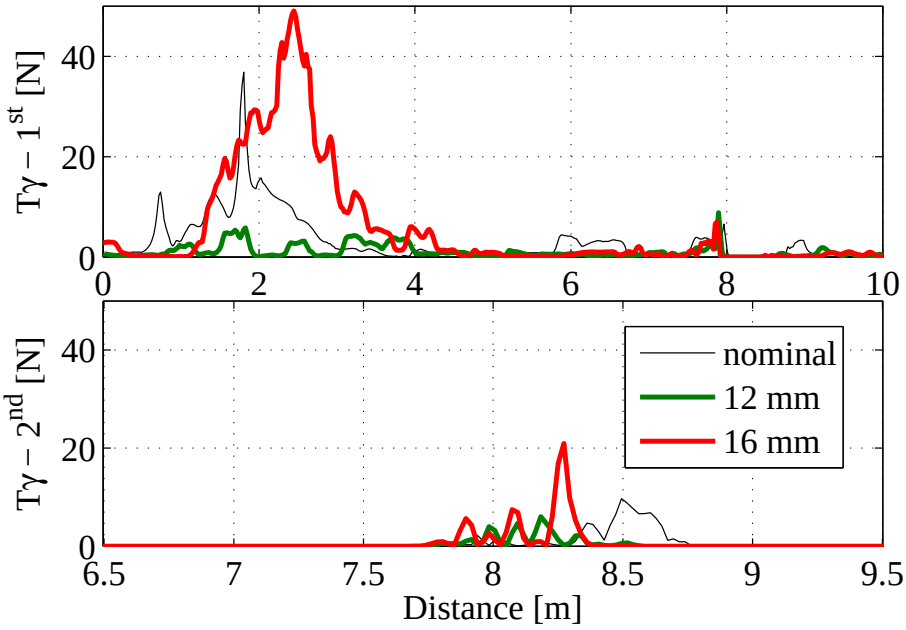

Figure 3.4. Wear indices ($T\gamma$) in the switch panel. First contact point (top) second contact point (bottom). Train in trailing move of through route

To further evaluate the optimum design, simulations were carried out using 18 measured wheel profiles. The performance of the optimal design was also assessed with respect to RCF. The engineering model for prediction of RCF impact developed by Ekberg et al. [3.4] was used. The surface-initiated RCF index FI_{surf} is expressed as

$$FI_{\text{surf}} = \frac{\sqrt{T_x^{\,2} + T_y^{\,2}}}{F_{\text{n}}} - \frac{2\pi abk}{3F_{\text{n}}} \qquad (1)$$

where F_{n} is the normal contact force, T_x and T_y are the creep forces in the longitudinal and lateral directions, a and b are the semi-axes of the Hertzian contact patch, and k is the yield limit in pure shear (here taken as 300 MPa). Surface-initiated RCF is predicted to occur if $FI_{\text{surf}} > 0$. Based on simulations with 18 different wheel profiles, the maximum FI_{surf} is shown in Figure 3.5. The limit for RCF prediction is exceeded at more locations for the nominal S&C design compared to the gauge optimised geometry.

Thus, with the adopted geometrical representation of gauge widening, the switch panel design corresponding to the 12 mm maximum gauge widening is the optimal design for the through route, both for the facing and trailing moves.

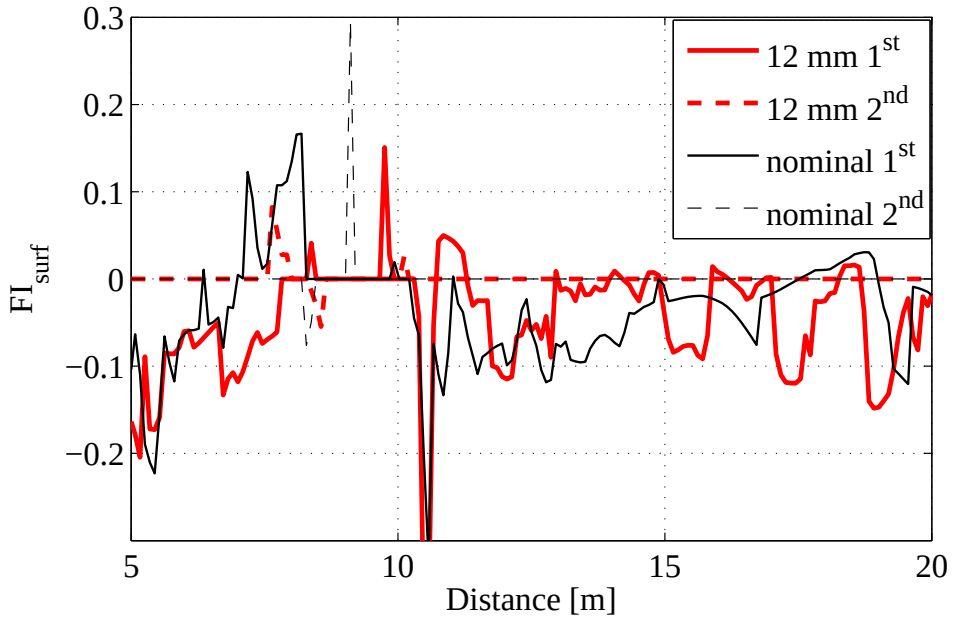

Figure 3.5. Maximum RCF index along the switch panel for the nominal and optimised geometry. Train in facing move of through route

3.2.2. Diverging route

The aim of the gauge variation is to relieve the flange contact on the switch rail at an early stage by steering the wheel towards the other rail. Here, three levels of maximum gauge increase {8 mm, 12 mm and 18 mm} were studied.

Based on simulations in the facing move for the nominal design and with dynamic gauge widening, Figure 3.6 shows the wear indices for

all gauge amplitudes in the switch panel for the first and second contact points. No significant improvement is obtained with respect to the wear index for any of the three levels of gauge widening amplitudes. Thus, another type of gauge widening geometry, with more design parameters, needs to be investigated to improve the design of the diverging route.

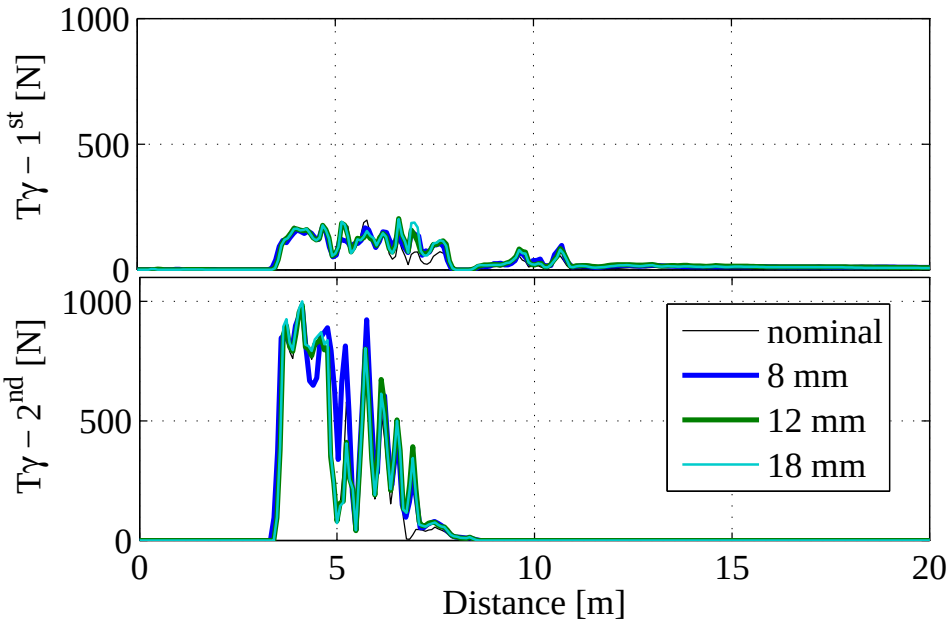

Figure 3.6. Wear indices ($T\gamma$) in the switch panel with three gauge widening amplitudes. First contact point (top), second contact point (bottom). Train in facing move of diverging route

3.3. Track stiffness optimisation

Measured track receptances, with single point excitation applied on the rail head of the switch and stock rails both in the vertical and lateral directions, have been used to characterise the track. The receptance was measured at several locations along a similar turnout at Härad in Sweden [3.2], and the values measured at three locations in the switch panel (4.5 m, 9.1 m and 21.85 m from the front of the S&C) were used to determine input data for a track model that was used to optimise the track stiffness in the switch panel.

Two track models have been compared, see Figure 3.7. The first model has three degrees-of-freedom (dof), while the second track model has seven dof with two additional masses incorporated to represent the rail masses and two spring-damper pairs to represent the combined rail and rail pad stiffness, see [3.1] for more detail. The

track model parameter values are varying along the switch panel. This is done by varying the values of the rigid masses and the spring-damper elements within the model.

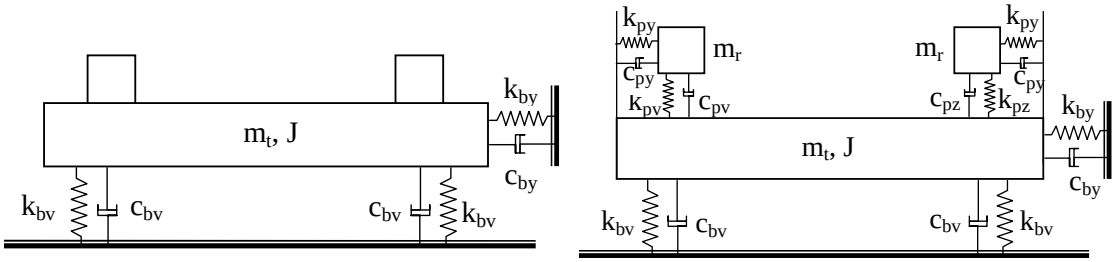

Figure 3.7. Moving track model with 3 dof (left) and 7 dof (right)

It was observed that the rail (and rail pad) stiffness at the second measurement location (9.1 m) was increased by 40% compared to the corresponding stiffness at measurement point 1 (4.5 m). The stiffness increased by 70% at the third measurement location (21.85 m) compared to the first point.

Vertical track receptance measured close to the front of the turnout (4.5 m) and the corresponding calculated receptances based on the two moving track models are illustrated in Figure 3.8. The first resonance is obtained at about 30 Hz. A second resonance is obtained at about 320 Hz. The magnitude of the calculated receptance is in good agreement with the measured receptance up to 400 Hz for the seven-dof model and up to 150 Hz for the three-dof model.

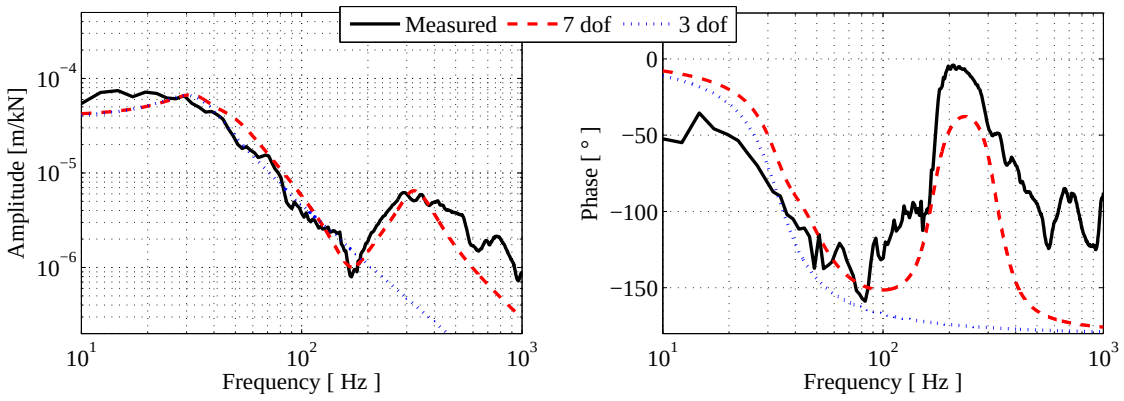

Figure 3.8. Calculated and measured vertical receptance amplitudes (left) and phase angle (right)

Compared to the track model that was tuned based on track receptance measurements, the value of the rail/rail pad stiffness (k_p) in the first stiffness optimisation model, (k_p_v1), was increased by 30% at location 1 and reduced by 15 % at location 3, keeping the value at location 2 unchanged. This gives rise to a smaller change of k_p-values along the switch panel: 416 MN/m, 448 MN/m, 462.4 MN/m at locations 1, 2 and 3, respectively. The stiffness values in the second model (kp_v2) leads to a further reduction of the stiffness increase between location 1 and location 3, down to about 8 %. This is obtained by increasing the value of k_p at location 1 by 28 % from the measured value, and reducing it by 6 % and 19 % at locations 2 and 3, respectively. This gives values of k_p at the three locations of 409.6 MN/m, 441.6 MN/m, and 454.4 MN/m. The stiffness variation is now relatively constant throughout the switch panel. This can be achieved by placing stiffer rail pads starting from some distance before the front of the turnout and softer rail pads close to the switch heel.

The optimisation was performed for one load case. The vehicle model was simulated in the facing move of the through route and with the three different track stiffness arrangements: nominal (k_p_nom), variation 1 (k_p_v1), and variation 2 (k_p_v2). Figure 3.9 shows the wear indices for the three stiffness variation cases. The maximum wear index for the second contact point (at about 8.2 m) for the nominal case is 10 N. A slight reduction is obtained, 9.3 N and 7.5 N, when using the k_p_v1 and k_p_v2, model arrangements, respectively.

Together with the k_p-variation, an optimisation of the spring-damper element stiffness for the sleeper/ballast structure (k_b) has also been considered. The k_b stiffness value was increased by 20% at location 1, reduced by 10% at location 2 and reduced by 20% at location 3, corresponding to 39 MN/m, 41 MN/m and 46.8 MN/m, respectively.

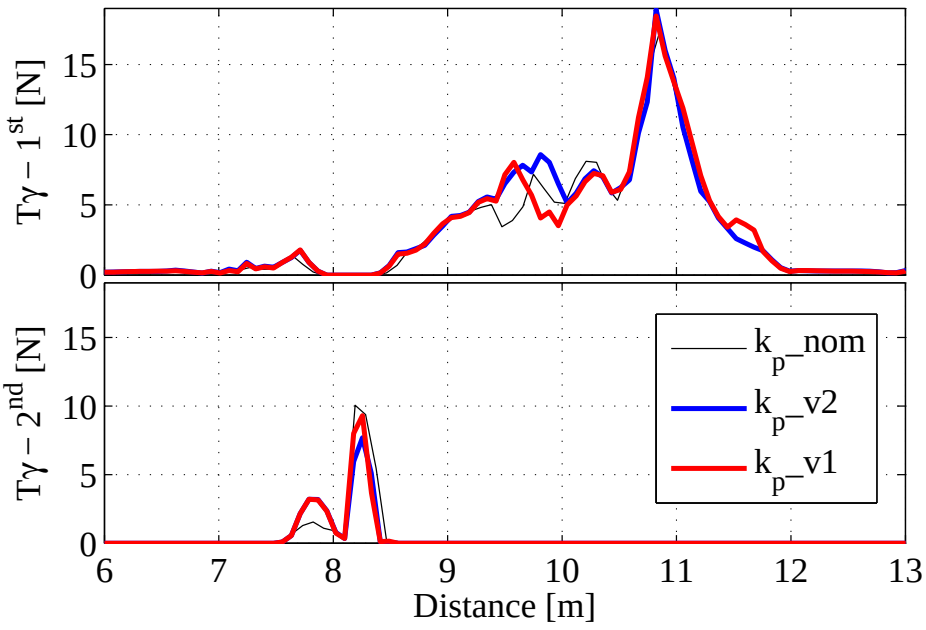

Figure 3.9. Wear indices ($T\gamma$) for three variations of k_p. First contact point (top), second contact point (bottom). Train in facing move of through route

Wear indices along the switch panel for different combinations of variations in k_p and k_b are shown in Figure 3.10. Maintaining the nominal k_p-values, while varying k_b, reduces the wear index at the second contact point by almost 50 %, from 10 N to 5.3 N. A relatively large reduction in the wear index is obtained when optimised k_p and k_b stiffness values are used in combination. The reduction is seen both at the first and second contact points. At the first contact point, the maximum wear index (at 10.7 m) is reduced by 50 % from 18.9 N to 9.5 N. The maximum wear index at the second contact is reduced by more than the sum of the individual reduction to only 2.2 N, i.e. an 80 % reduction is obtained.

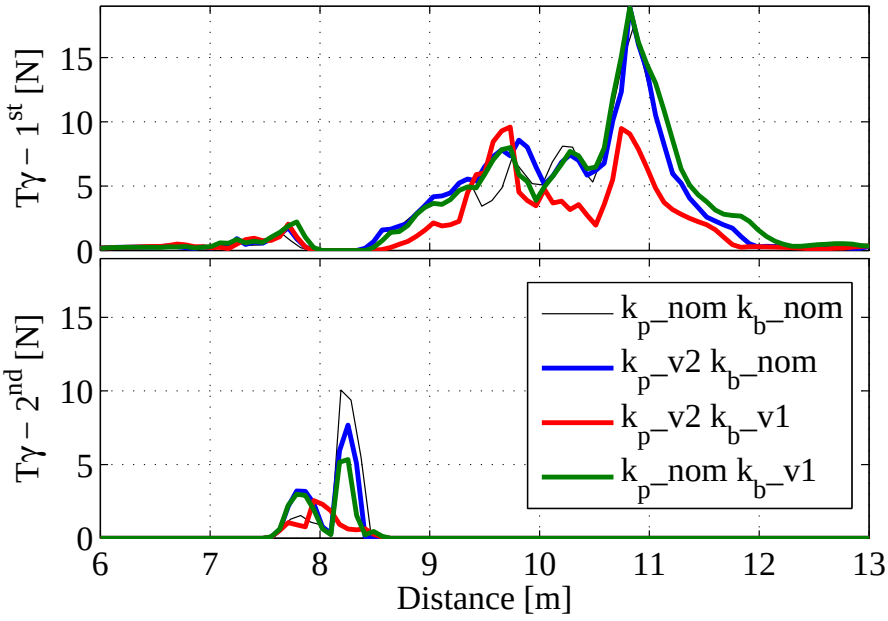

Figure 3.10. Wear indices ($T\gamma$) with combinations of variations in k_p and k_b. First contact point (top), second contact point (bottom). Train in facing move of through route

3.4. Recommendation

Based on the performed simulations, it has been shown that the application of gauge widening in the switch panel has a strong potential in reducing wear and RCF.

The proposed geometry modification with a widening of the gauge at switch entry could relieve the flange contact with the switch rail at the early stage by steering the wheel towards the other rail. In addition, with this geometry modification, the tip of the switch rail could be thicker which gives more material for wear and hence reduces LCC for the switch.

The optimisation process was performed for a standard S&C design (UIC60-760-1:15) with curve radius 760 m. The optimal gauge widening amplitude for this design is 12 mm resulting in an improved performance. The results may not be directly applicable to other designs; however, the conclusion could give a good approximation. The same methodology can be applied to other S&C designs. The geometry modification can easily be incorporated into new designs without extra cost. It can also be incorporated in

existing designs without further investigation as the maximum gauge variation (12 mm) could be within the tolerance limit.

For track stiffness optimisation, two alternative stiffness variation models were considered. The influences on wear index and wheel-rail contact forces were investigated. The stiffness variation is expected to be achieved by varying the rail pad stiffness along the switch panel and by applying under sleeper pads. Placing stiffer rail pads starting from some distance before the front of the turnout and softer rail pads close to the switch heel can improve the smoothing of the large change in track stiffness along the switch panel. A considerable reduction in wear index is obtained (up to 80% on the peak value) when varying the k_p stiffness by a maximum of ±30% and k_b stiffness values by a maximum of ±20%.

3.5. Future work

The gauge optimisation presented here was based on the position of the contact point jump location for one type of traffic (freight vehicle with Y25 bogies). However, in practice, for the same turnout geometry design, the position of the contact point jump varies a lot due to several variables related to different types of passing train. Therefore, the outcome of this study should be taken as a preliminary result, and a more thorough analysis including other load cases and scatter in load conditions should be considered in the optimisation process. The optimisation process assumed only one type of gauge widening geometry with a single variable (maximum gauge widening). Other types of gauge widening geometry, with more design variables, could be investigated.

The track model used here is not sufficient to carry out a comprehensive track stiffness optimisation exercise. One deficiency of the present track model is that the interaction of adjacent wheelsets, through the rail, is not accounted for. In addition, the flexibilities of the different components (rail and rail pad) are lumped into a single stiffness value, and its variation along the switch is not well represented. Therefore, a more advanced track model, based on an FE model that can describe all the different flexible components and represent the stiffness variation along the turnout more accurately, see for example [3.5], is required.

Only an optimisation of vertical track stiffness was covered in this study. An optimisation of lateral track stiffness could also be

performed, mainly for the diverging track. In addition, different countries adopt different rail inclinations in turnouts. The influence of rail inclination could also be investigated to identify an optimum inclination.

3.6. Bibliography

3.1 E Kassa, S Iwnicki, J Perez, P Allen, Y Bezin, Optimisation of track gauge and track stiffness along a switch using a multibody simulation tool, to be published in the Proceedings of the 21st International Symposium on Dynamics of Vehicles on Roads and Tracks, Stockholm, Sweden, August 17 – 21, 2009, 12 pages

3.2 E Kassa and J C O Nielsen, Data from field test in turnout in Härad, INNOTRACK Technical report, 19 pp, June 2007

3.3 J Perez, Optimisation of the dynamic gauge for railway switches, INNOTRACK Technical report, December 2008, 25 pp (Appendix C in D3.1.4)

3.4 A. Ekberg, E. Kabo, and H. Andersson, An engineering model for prediction of rolling contact fatigue of railway wheels. *Fatigue & Fracture of Engineering Materials & Structures*, 25(10), p. 899-909, 2002

3.5 E. Kassa and J.C.O. Nielsen, Dynamic train-turnout interaction in an extended frequency range using a detailed model of track dynamics. *Journal of Sound and Vibration*, 320(4-5), p. 893-914, 2009

4. Optimisation of stiffness and geometry in the crossing panel

4.1. Background

One objective of INNOTRACK SP3.1 is to optimise the transition geometry and support stiffness of the superstructure in order to minimise the material degradation induced by wheels passing the frog (crossing nose and wing rails). For this purpose, the influence of different system parameters on impact loads generated on a German standard crossing EH 60-500-1:12 has been studied. Several alternative frog geometries have been investigated.

The simulations were carried out by DB Systemtechnik using the MBS package SIMPACK. Because of the higher speed and consequently higher impact loads compared to the diverging route, only the through route of the turnout was considered.

The influence of operational and service conditions was studied by varying the following parameters:

- static wheel load,
- speed,
- wheel profile,
- initial lateral wheel position at crossing entry,
- track stiffness, unsupported sleepers,
- running direction (facing and trailing move).

The simulations were performed with complete 3-dimensional vehicle models of a Loco BR 101 and of an ICE-T coach (BR 411), representing two different wheel loads (Loco BR 101: Q_0 = 107 kN, ICE-T coach: Q_0 = 67 kN). Three different wear states of the wheel profiles were used: nominal S1002, medium-worn and hollow worn. The track was represented by a finite element model (FEM) consisting of elastic rails and elastically supported elastic sleepers. More details are given in [4.1].

The investigation was based on the assumption that the maximum normal wheel-rail contact force is representative for the material degradation of the frog. To verify this approach, it was decided to use Kalker's CONTACT program for additional calculations of the

maximum contact stresses for some selected load cases. The result of Kalker's linear-elastic material model is the 3-dimensional stress state within the discretised contact patch from which the equivalent von Mises stress has been determined, for details see [4.2].

4.2. Optimisation of transition geometry

Regarding the optimisation of transition geometry of rigid (non-movable) crossings, two general approaches have been studied. The first one has the target to prevent the wheel from making contact with the crossing nose at a section being too weak to withstand the impact loads. The second approach aims at smoothing the vertical wheel movement during the transition between wing rail and crossing nose to reduce the impact loads. Based on these approaches the following solutions were investigated by simulations:

- Reduction of the flangeway width between crossing nose and wing rail within the allowed tolerances in order to delay the transition area to a thicker cross-section of the crossing nose;
- Profiling of the frog by following a kinked ramp to decrease the gradient of the vertical wheel movement after transition to the crossing nose (optimisation for facing move);
- Superelevation of the wing rail and profiling with a negative wheel shape to reduce the vertical wheel movement (MaKüDe).

Examples of the improved curves of the vertical wheel movement compared to what is obtained for the nominal frog geometry are shown in Figure 4.1. This figure also contains a short version of the kinked ramp which has the same effect on the impact loads in the transition area as the longer version.

Furthermore, another modification of the nominal crossing design was investigated which was initiated by the known problem of wing rail damage caused by hollow worn wheels passing in the trailing move. In trailing move, the outer section of a hollow worn wheel arrives too deep and hits the gauge corner of the wing rail. To avoid this, a small chamfer was added on the wing rail flange to reduce the contact angle when the wheel is transferred to the wing rail. This effect is illustrated in Figure 4.2. More details regarding the investigated designs can be found in [4.1].

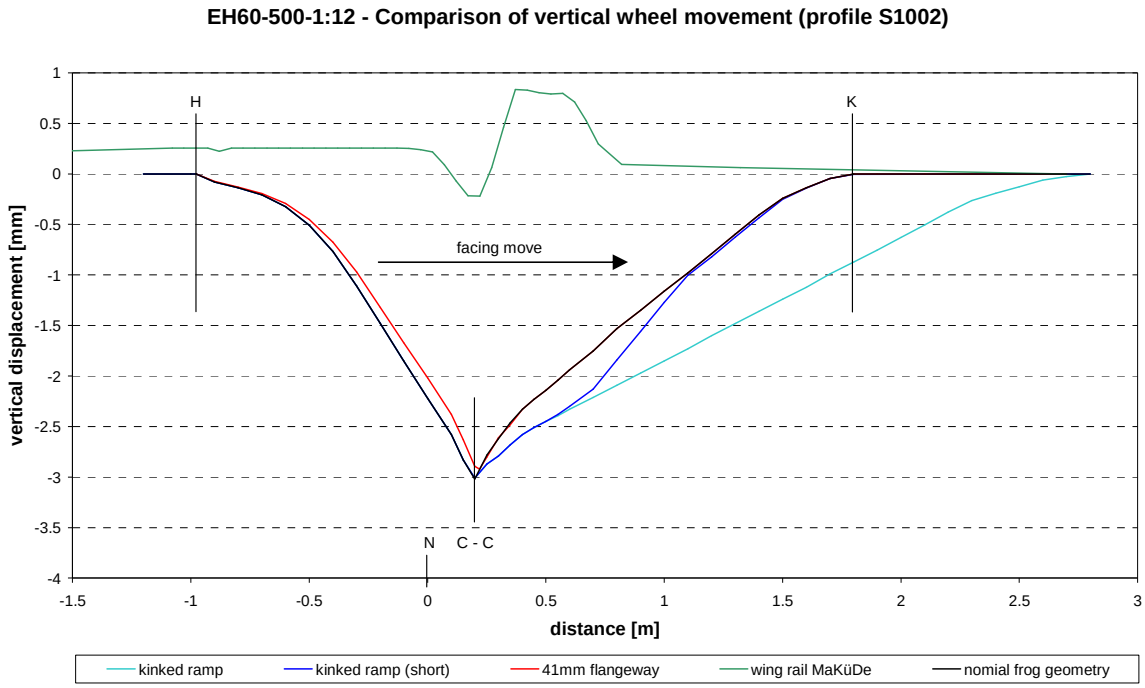

Figure 4.1: Influence of geometric frog design on vertical wheel movement, with point N indicating the tip of the crossing nose (s = 0 m)

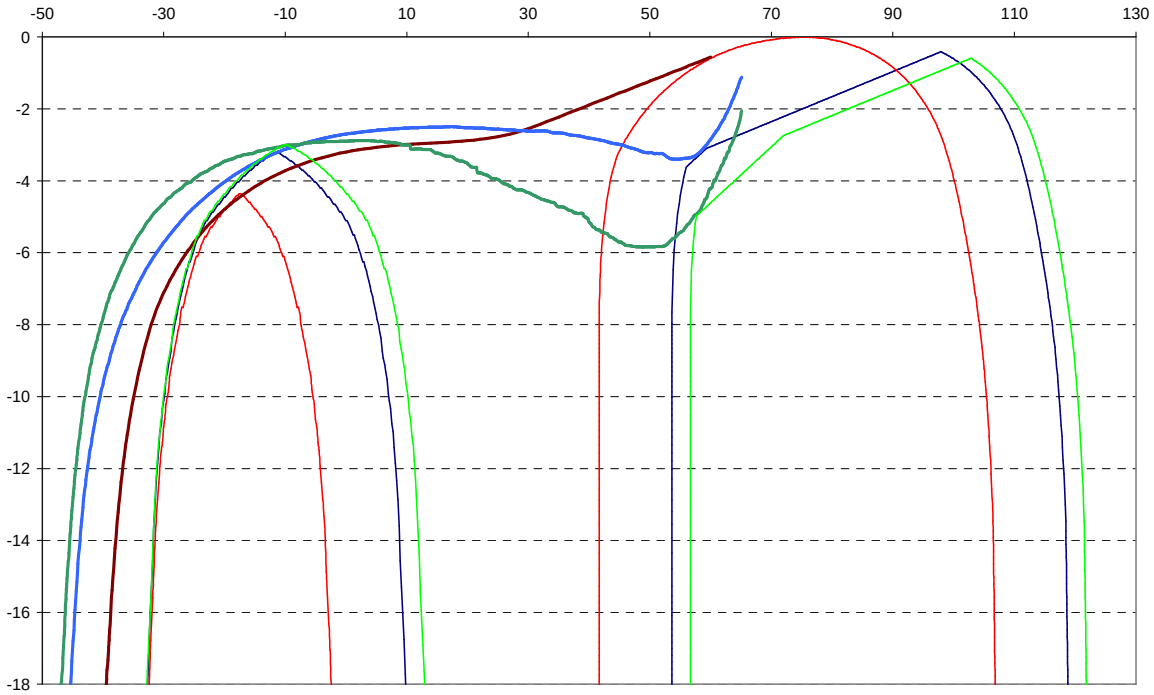

Figure 4.2: Contact situations at the point of wheel transition for new and hollow -worn wheel profiles on a chamfered wing rail. The severely worn wheel (green thick line) will be transferred at the green cross-section with a deep chamfer, the moderately hollow worn wheel (blue thick line) at the blue cross-section with a shallow chamfer and the new wheel (brown thick line) at the nominal transition point represented by the red cross-section

4.3. Simulation results

In the following, the most important simulation results are presented. More details can be found in [4.1] and [4.2].

The results of the investigation regarding track stiffness are illustrated in Figure 4.3. An interesting result is that a reduction of track stiffness from 500 kN/mm to 85 kN/mm, due to the use of elastic rail pads, leads to significantly lower normal contact forces and an increasing effect with increasing speed. Also in the case of one unsupported sleeper below the transition area of the crossing, slightly reduced impact loads can be observed. Thus the modification of track stiffness in the crossing panel indicates a high potential for reduction of material degradation of frogs.

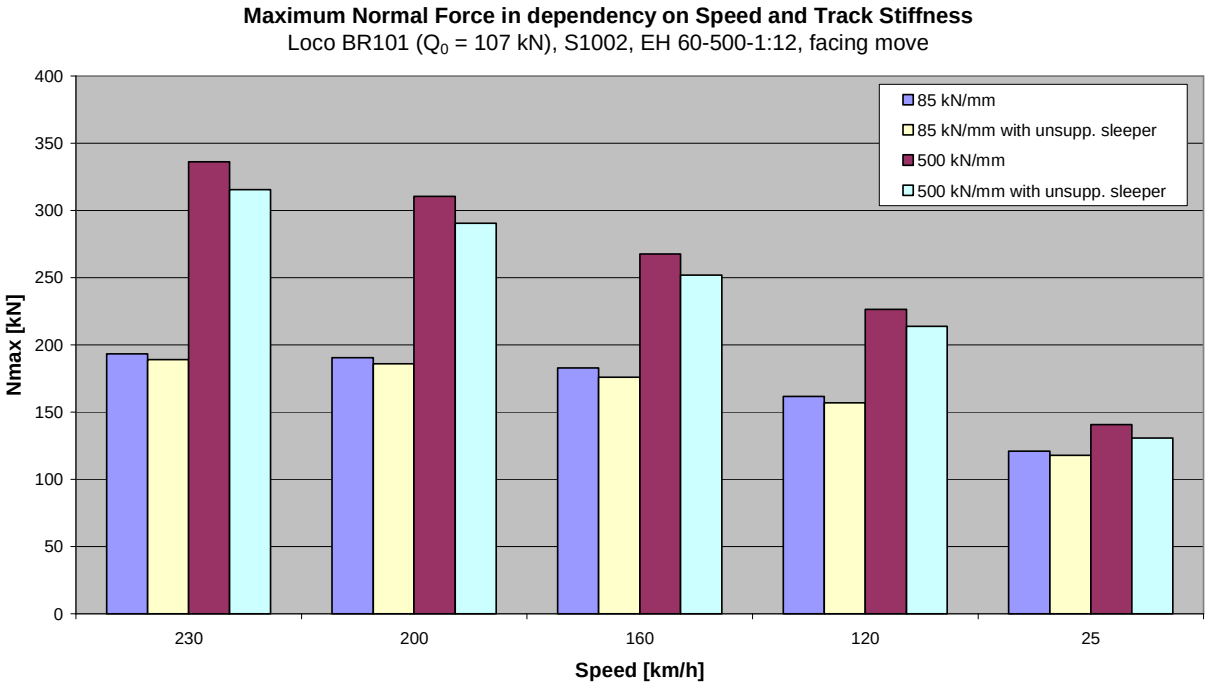

Figure 4.3: Influence of train speed and track stiffness on the maximum normal contact force

Maximum normal contact forces and maximum equivalent stresses for the alternative crossing designs are presented in Figure 4.4. For the theoretical S1002 wheel profile, the biggest force reduction (up to 50 kN) can be reached with the kinked ramp design whereas the MaKüDe design leads to even higher normal contact forces than the nominal design. This is caused by the steep gradient of the wheel movement after transition to the frog, see Figure 4.1. For worn wheels, the effect is inverted. Here the MaKüDe design provides by far the lowest normal contact forces. For the medium-worn wheel

profile, the MaKüDe design leads to a peak force reduction of nearly 50 %.

Looking at the calculated equivalent von Mises stresses, different trends than for the normal contact forces can be observed. The reason is that the maximum normal contact force usually occurs at a different location than the maximum equivalent stress because, due to the differences of the rail profile geometry, at some locations relatively low normal forces may cause very high stresses and vice versa, see Figure 4.5. Hence, small changes of contact conditions (contact radii) may lead to big variations in contact stresses. Only for the MaKüDe design passed by worn wheels, both an evaluation in terms of maximum normal contact force and equivalent contact stress lead to the same conclusion. In this case, the MaKüDe design provides the best performance with respect to both criteria.

It should be noted that the contact stresses are evaluated from simulations featuring a linear-elastic material model. Calculated stress values higher than the yield limit are unrealistic and indicate that in reality plastic deformation will occur. Consequently, in practice, a quick adaptation of the rail shape will be observed at these positions of the crossing leading to a significant stress reduction. In parallel, strain hardening will increase the resistance of the frog material. Thus, for practical applications, it seems to be more relevant to compare impact forces than linear-elastic contact stresses.

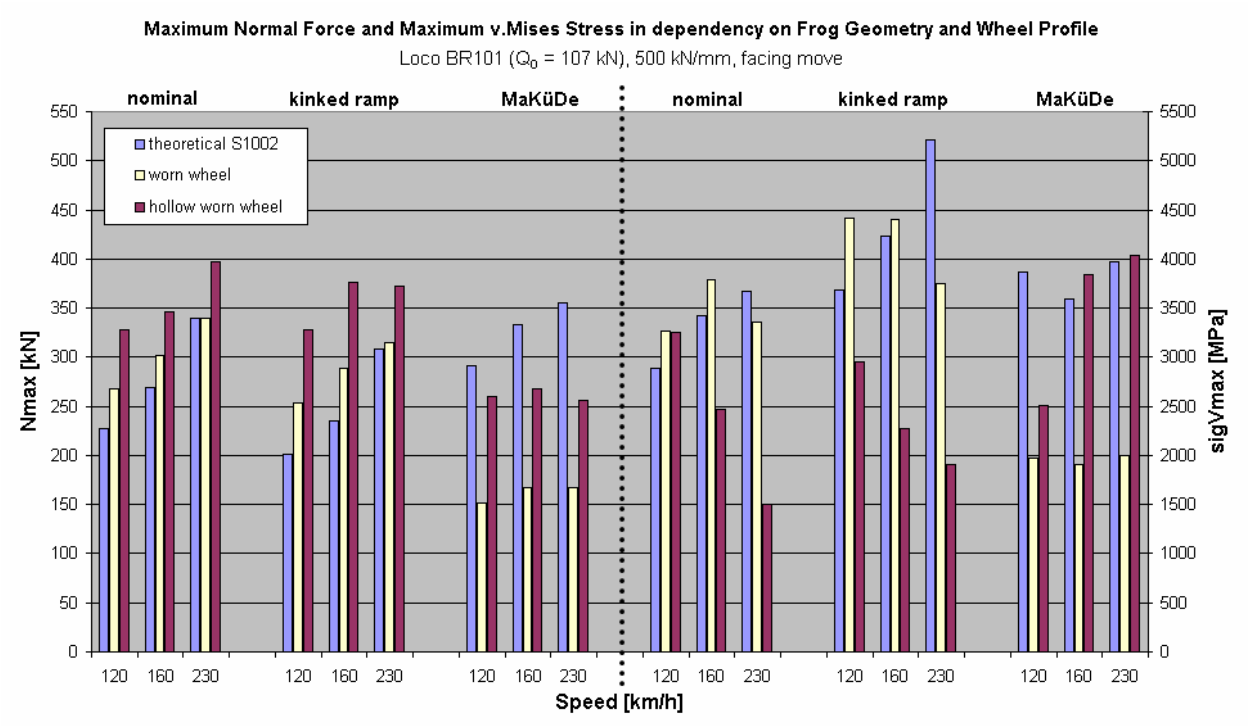

Figure 4.4: Influence of transition geometry and wheel profile on maximum normal contact force and equivalent stress

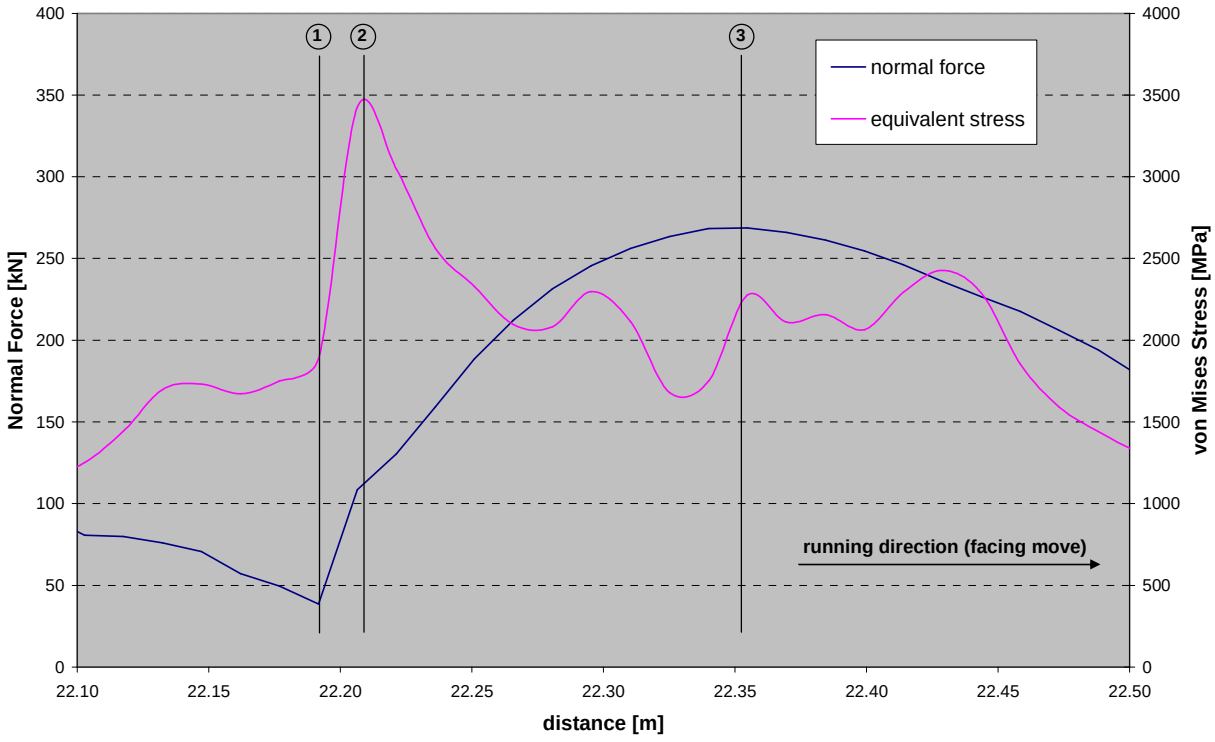

Figure 4.5: Normal contact force evaluated for a Loco BR 101 passing at v = 160 km/h with wheel profile S1002 in centred position (1 – wheel transition from wing rail to frog, 2 – maximum equivalent stress, 3 – maximum normal force)

4.4. Conclusions and recommendations

For a German rigid frog EH 60-500-1:12, the influence of different system parameters on the impact loads has been studied by means of MBS simulations with SIMPACK. The investigation was focused on the vertical track stiffness in the crossing panel and on the transition geometry which is represented by the vertical wheel movement when passing the crossing.

It was shown that impact loads can be reduced considerably, especially for crossings passed at high speed, if a reduced support stiffness is introduced by means of elastic rail pads. However, it has to be considered that the possible softening of the elastic foundation may be limited due to potential fatigue of the rail foot caused by bending.

Furthermore, several crossing geometries were investigated to find an optimal geometric design for the crossing nose and wing rails. The calculation results illustrate that it is difficult, if not impossible, to find a solution which leads to a force reduction for all wheel profiles occurring in service. Nevertheless, the MaKüDe design developed by DB Systemtechnik showed the best performance for moderately worn wheel profiles in both running directions (facing and trailing moves). In connection with reduced support stiffness (e.g. elastic rail pads), this crossing design will lead to a significant reduction of impact loads and consequently provide a high potential of LCC reduction.

4.5. Future work

The investigation of contact stresses on crossings calculated by means of Kalker's CONTACT program has demonstrated the limited usefulness of linear-elastic material models in this field of application. On the other hand, considering only maximum contact forces with regard to material degradation on frogs could lead to invalid conclusions. Before carrying out expensive in-field tests, the most promising frog designs could be investigated by means of the simulation methodology [4.3] developed by Chalmers University of Technology to evaluate frog degradation in terms of plastic deformations and wear.

4.6. Bibliography

4.1 D. Nicklisch, SIMPACK-simulations of passing switches and crossings, INNOTRACK Technical report, December 2008, 11 pp and two appendices (Appendix D in D3.1.4)

4.2 D. Nicklisch, SIMPACK-simulations of contact stresses on switches and crossings, INNOTRACK Technical report, July 2009, 8 pp and two appendices

4.3 A. Johansson, B. Pålsson, M. Ekh, J. C. O. Nielsen, M. K. A. Ander, J. Brouzoulis and E. Kassa, Simulation of wheel-rail contact and damage in switches and crossings, To be published in the Proceedings of the 8th International Conference on Contact Mechanics and Wear of Rail/Wheel Systems, Firenze, Italy, September 15 – 18, 2009

5. Conclusions

The presented numerical simulations show that a significant reduction of wear and RCF on the through route of S&C can be achieved by applying a dynamic gauge widening at the switch entry. The gauge optimisation process was based on varying a single variable (maximum gauge widening), which represented the gauge optimisation geometry. Several gauge widening amplitudes were analysed. Large gauge amplitudes lead to larger displacements to the other side of the track, which cause the wheelset to exhibit additional lateral excitation. The geometry with 12 mm gauge widening amplitude resulted in an improved performance, both in the facing and trailing moves of the through route. This was validated by running several simulations with a wide set of load cases to prove that this is an optimal design. The optimised geometry showed more consistency in the results (significant reduction of wear and RCF indices compared to the nominal design) when using different wheel profiles.

The gauge optimisation is assumed for a given contact point jump location. However, in practice, for the same turnout geometry design, the contact point jump varies due to several variables related to the different types of passing train. Therefore, future work is intended to develop a systematic approach of the novel dynamic gauge widening technique that will be valid for all S&C designs and that takes into account the scatter in the loading conditions.

For track stiffness optimisation, two alternative stiffness variation models were considered. The maximum variations of the track stiffness at the three locations were limited to ±30 %. This is expected to be achieved by varying rail pad stiffness and by applying under sleeper pads. The influence on wear index and wheel-rail contact forces was investigated. Optimising only the rail/rail pad stiffness (k_p) value shows a slight reduction in the maximum wear index. Optimising only the sleeper/ballast stiffness (k_b) value leads to a reduction of the wear index by almost 50% for the switch rail contact while the change for the stock rail contact is minimal. A considerable reduction in the wear index is obtained (up to 80%) when both the k_p and k_b stiffness values are optimised. However, no

significant change in normal contact force is obtained for any of the track stiffness optimised models.

The assessment of a crossing panel with reduced support stiffness (by means of elastic rail pads) instead of the standard support stiffness showed that impact loads can be reduced considerably especially for crossing negotiation at high speed. Investigations of different crossing geometries showed that it is difficult to find a solution that leads to a force reduction for all wheel profiles occurring in service. Nevertheless, the MaKüDe crossing design showed the best performance for moderately worn wheel profiles in both running directions (facing and trailing moves). In combination with reduced support stiffness, this crossing design should lead to a significant reduction of the impact loads and consequently has a high potential for LCC reduction.

6. Annexes

Elias Kassa, Simon Iwnicki, Javier Perez, Paul Allen and Yann Bezin, Optimisation of track gauge and track stiffness along a switch using a multibody simulation tool, to be published in the Proceedings of the *21st International Symposium on Dynamics of Vehicles on Roads and Tracks*, Stockholm, Sweden, August 17 – 21, 2009, 12 pages (Appendix A in D3.1.5)

Dirk Nicklisch, SIMPACK-simulations of contact stresses on switches and crossings, Report 06-P-4798-TZF63-INNOTRACK, Deutche Bahn AG, Systemverbund Bahn – Technik, DB Systemtechnik, July 2008, 8 pp and two appendices (Appendix B in D3.1.5)